Murat Alp Oztek, MD [*]
Nina A. Mayr, MD [‡]
Mahmud Mossa-Basha, MD [*]
Matthew Nyflot, PhD [*‡]
Patricia A. Sponseller, MS, CMD, RT(R)(T) [‡]
Wei Wu, MD [*]
Christoph P. Hofstetter, MD [§]
Rajiv Saigal, MD, PhD [§]
Stephen R. Bowen, PhD [*‡]
Daniel S. Hippe, MS [*]
William T. C. Yuh, MD, MSEE [*]
Robert D. Stewart, PhD [‡]
Simon S. Lo, MD [‡]

[*]Department of Radiology, University of Washington School of Medicine, Seattle, Washington; [‡]Department of Radiation Oncology, University of Washington School of Medicine, Seattle, Washington; [§]Department of Neurological Surgery, University of Washington School of Medicine, Seattle, Washington

Preliminary results of this study were presented at the Radiological Society of North America (RSNA) 104th Scientific Assembly and Annual Meeting, November 25-30, 2019 in Chicago, Illinois, and at the 2019 Radiosurgery Society Annual Scientific Meeting, March 21-23, 2019, in San Diego, California.

Correspondence:
Nina A. Mayr, MD,
Department of Radiation Oncology,
University of Washington Medical Center,
1959 NE Pacific St, Box 356043,
Seattle, WA 98195, USA.
Email: ninamayr@uw.edu

Received, September 17, 2019.
Accepted, March 19, 2020.
Published Online, June 4, 2020.

The Dancing Cord: Inherent Spinal Cord Motion and Its Effect on Cord Dose in Spine Stereotactic Body Radiation Therapy

BACKGROUND: Spinal cord dose limits are critically important for the safe practice of spine stereotactic body radiotherapy (SBRT). However, the effect of inherent spinal cord motion on cord dose in SBRT is unknown.

OBJECTIVE: To assess the effects of cord motion on spinal cord dose in SBRT.

METHODS: Dynamic balanced fast field echo (BFFE) magnetic resonance imaging (MRI) was obtained in 21 spine metastasis patients treated with SBRT. Planning computed tomography (CT), conventional static T2-weighted MRI, BFFE MRI, and dose planning data were coregistered. Spinal cord from the dynamic BFFE images ($cord_{dyn}$) was compared with the T2-weighted MRI ($cord_{stat}$) to analyze motion of $cord_{dyn}$ beyond the $cord_{stat}$ (Dice coefficient, Jaccard index), and beyond $cord_{stat}$ with added planning organ at risk volume (PRV) margins. Cord dose was compared between $cord_{stat}$, and $cord_{dyn}$ (Wilcoxon signed-rank test).

RESULTS: Dice coefficient (0.70-0.95, median 0.87) and Jaccard index (0.54-0.90, median 0.77) demonstrated motion of $cord_{dyn}$ beyond $cord_{stat}$. In 62% of the patients (13/21), the dose to $cord_{dyn}$ exceeded that of $cord_{stat}$ by 0.6% to 13.8% (median 4.3%). The $cord_{dyn}$ spatially excursed outside the 1-mm PRV margin of $cord_{stat}$ in 9 patients (43%); among these dose to $cord_{dyn}$ exceeded dose to $cord_{stat}$ + 1-mm PRV margin in 78% of the patients (7/9). $Cord_{dyn}$ did not excurse outside the 1.5-mm or 2-mm PRV cord $cord_{stat}$ margin.

CONCLUSION: Spinal cord motion may contribute to increases in radiation dose to the cord from SBRT for spine metastasis. A PRV margin of at least 1.5 to 2 mm surrounding the cord should be strongly considered to account for inherent spinal cord motion.

KEY WORDS: Ablative radiotherapy, Motion, MR imaging, Organ motion, Patient positioning, Secondary spine metastasis, Spinal cord, Spinal cord physiology, Spinal neoplasms, Stereotactic radiation therapy

Neurosurgery 87:1157–1166, 2020 DOI:10.1093/neuros/nyaa202 www.neurosurgery-online.com

Metastases to the spine are a common complication of cancer, occurring in up to 40% of cancer patients,[1,2] and can result in major functional morbidity, including pain, pathological vertebral fractures, myelopathy, and radiculopathy from compression of adjacent neural structures.[3]

ABBREVIATIONS: AP, anteroposterior; **BFFE,** balanced fast field echo; **CSF,** cerebrospinal fluid; **CT,** computed tomography; **LQ,** linear quadratic; **MRI,** magnetic resonance imaging; **PRV,** planning organ at risk volume; **PTV,** planning target volume; **SBRT,** stereotactic body radiotherapy

Supplemental digital content is available for this article at www.neurosurgery-online.com.

With the rapid advancement in the precision of imaging and radiation therapy delivery, spine stereotactic body radiation therapy (SBRT) has become an effective noninvasive treatment option for realistic long-term local disease control, maintenance of neurological function, and pain relief in spine metastasis patients.[4,5]

The spinal cord is the major radiation dose-limiting tissue in spine SBRT, and the risk of irreversible neurological deficits from radiation myelopathy remains a feared complication of this treatment.[6-9] For the safe practice of spine SBRT, dose constraints have been established for the spinal cord.[2,5,7,10,11] However, the definition of the spinal cord as a planning organ at risk volume (PRV) has varied considerably with no consensus regarding the use of safety margins

(PRV expansions) around the cord to account for setup uncertainties, contouring variations, and organ motion. In clinical practice, PRV expansions have ranged from no expansion to 1.5- to 2-mm PRV margins.[12] While the high-precision delineation of the spinal cord and its spatial relationship to the spinal tumor is now generally performed on high-resolution T2-weighted magnetic resonance images, the dose effects from inherent motion of the spinal cord have not been considered in the SBRT plan design and dosimetry process.

Physiological motion of cerebrospinal fluid and spinal cord during the cardiac and respiratory cycle has been well described in normal subjects and patients with nonmalignant spine conditions. However, the inherent motion pattern of the cord in spine tumor patients has been less well understood. A recent study by Tseng et al,[13] using precision MRI-based delineation of the cord, demonstrated, for the first time, significant spinal cord motion in spine SBRT patients. The impact of the cord's motion on the dose received by the cord, however, remains unknown.

Because the cord is generally located within millimeter distance from the planning target volume (PTV) and thereby subjected to the very sharp dose gradients of ablative SBRT to the tumor,[5,8,14,15] even minimal cord motion may exert a significant effect on the actually received dose to the spinal cord and its vulnerable serial microstructures. There is an unmet need to recognize the potential physiological motion of the "dancing" (ie moving) cord and quantify its dose effect on the cord, particularly for patients with limited cord tolerance due to close proximity of the target to the cord and/or prior spine radiation.

The purpose of this research was to evaluate the pattern of inherent spinal cord motion for SBRT of spine metastases, and assess the effects of cord motion on the dose received by the cord. Our specific aims were to quantitate the cord's motion by dynamic MRI, and compare the dosimetric parameters between the moving ("dancing") and static cord defined by the conventional static T2-weighted MRI. Our ultimate goal was to derive recommendations for PRV margins that take into account the effects of spinal cord motion.

TABLE 1. Patient and Treatment Characteristics

Characteristic	No. of patients	Percentage
Tumor location		
C-spine	3	14
T-spine	17	81
L-spine[a]	1	5
Epidural spinal cord compression (Bilsky) grade		
0	5	24
1a	2	10
1b	7	33
1c	3	14
2	4	19
Primary tumor and histology[b]		
Breast carcinoma	4	19
Prostate carcinoma	3	14
Thyroid carcinoma	3	14
Gynecologic tumor[c]	3	14
Hepatocellular carcinoma	2	10
Renal cell carcinoma	2	10
Sarcomatous tumor[d]	2	10
Lung carcinoma	1	5
Pheochromocytoma	1	5
Fractionation schedule		
3-Fraction regimen	11	52
5-Fraction regimen	10	48
Distance between PTV and cord PRV (in mm)		
0	20	95
>0[e]	1	5

PTV = planning target volume.
[a]The L-spine lesion was at the level of the spinal cord.
[b]All patients had biopsy-proven malignancies.
[c]Two patients with uterine and one patient with ovarian carcinoma.
[d]One patient with extremity sarcoma and one patient with malignant schwannoma.
[e]In one patient the closest distance between cord PRV and PTV was 0.7 mm. The mean percentage of the $cord_{stat}$ dose relative to the prescription dose (using EQD2 with a α/β ratio of 2 Gy and 10 Gy, respectively) was 59.4 (±23.5)%.
Among the initially identified 25 consecutive patients with spinal metastases, 4 were excluded: 3 for spinal lesions below the conus and 1 in whom dynamic MRI was taken at a level without tumor. This resulted in 21 patients, age 37–88 (mean, 64) years, that constitute the study cohort.

METHODS

Study Design and Patient Population

This retrospective study included 21 adult patients with intact spinal metastases (treated October 2017 to March 2019). The study was approved by the Institutional Review Board, including consent waiver. All patients had dosimetry planning and an SBRT-tailored MRI protocol including a dynamic MRI sequence to study spinal cord motion. Patient characteristics are presented in Table 1.

Clinical Imaging and Treatment Planning

All patients underwent standard SBRT planning CT and spine-SBRT-tailored 3 Tesla MRI, including cardiac-gated dynamic balanced fast field echo (BFFE) MRI to assess spinal cord motion. For the BFFE MRI, 15 dynamic images were acquired over 2.5 to 5 min (depending on heart rate) for a total of 315 images in the 21 patients. Details of imaging are presented in Table 2.

For SBRT planning, target and normal tissue contouring had been previously performed based on rigid coregistration of simulation CT and conventional T2-weighetd MRI using MIM (v6.7.11, MIM Software, Cleveland, Ohio). Details of imaging and imaging use for target and normal tissue contouring are presented in Table 2. A PRV margin of 2 mm was added to the cord to derive the spinal cord PRV. Routine dosimetry was performed (dose calculation grid size 2 mm). Volumetric-modulated arc therapy was used in 20 patients and fixed-field intensity-modulated radiation therapy in 1 patient. PTV dose and normal tissue constraints were prescribed per routine SBRT dosing standards. The

TABLE 2. Planning Imaging and Use of Imaging for SBRT Target and Normal Tissue Delineation

Simulation CT	Noncontrast, 1.25-mm slice thickness		
SBRT planning use/delineation	CTV[a], PTV[b] normal structures (eg, esophagus, pharynx, larynx, bowel, lung), except spinal cord		
MRI	Sagittal 3D T2 turbo spin echo DRIVE sequence (3D TSE T2 DRIVE[c])	Sagittal fat-saturated 3D T1 gradient recalled echo 3D T1 THRIVE[d]	3D cardiac-gated dynamic balanced fast field echo (BFFE)[e]
TR/TE (ms)	1500/100	4.7/2.3	4.7/2.4
Matrix	300 × 245	296 × 186	172 × 171
Field of view (mm)	240 × 200 × 156	250 × 158 × 240	120 × 120 × 75
Resolution (acquired) (mm)	0.8 × 0.8 × 1.6	0.8 × 0.8 × 1.6	0.7 × 0.7 × 10
Resolution (interpolated) (mm)	0.8 × 0.8 × 0.8	0.8 × 0.8 × 0.8	–
Slices	98	150	5
Plane of acquisition	Sagittal	Sagittal	Axial
SBRT planning use/delineation	Spinal cord and GTV[f]	GTV[f]	Qualitative review[g]

Immobilization for CT: VacQfix (Qfix, Avondale, PA) or Bodyfix (Elekta, Stockholm, Sweden).
MRI: Philips 3.0 Tesla Ingenia (Philips Healthcare; Best, the Netherlands), standard spine coil.
[a]CTV = clinical target volume.
[b]PTV = planning target volume.
[c]DRIVE = driven Equilibrium.
[d]THRIVE = T1-weighted high-resolution isotropic volume examination.
[e]BFFE: 15 cardiac cycles triggered from peripheral pulse transducer.
[f]GTV = gross tumor volume.
[g]The review for image quality of the BFFE was carried out immediately after imaging acquisition. Imaging with inadequate quality secondary to motion or other factors was repeated or excluded.

maximal pixel dose to the spinal cord PRV was constrained to 20 Gy in the 3-fraction (11 patients) and to 25 Gy in the 5-fraction regimen (10 patients, Table 1).

Image Evaluation and Spinal Cord$_{dyn}$ Contouring

All imaging was coregistered using a research platform within MIM v6.7.11 (Figure 1), and coregistrations were independently reviewed by 2 investigators with extensive SBRT experience (co-authors S.S.L. and N.A.M.). The spinal cord (cord$_{dyn}$) was contoured on the each of the 15 dynamic BFEE images and on the static 3D turbo spin echo DRIVE T2-weighthed images (cord$_{stat}$) by one reviewer, and uncertainties were resolved in consensus with an additional reviewer. CT simulation image data sets with the treatment plans were coregistered to transfer existing dose data from the previous clinical treatment plan to the BFFE images. On the static images, 1, 1.5, and 2-mm expansions of the cord$_{stat}$ contour were created as shown in Figures 1A and 1B.

Dosimetric Analysis

Based on the coregistered BFFE, static T2-weighted MRI, planning CT, and dose data sets, we measured the pixel maximum dose (dose$_{max}$) to the cord, using the BFFE and corresponding static T2-weighted images at the level of the tumor lesion. The dose$_{max}$ to the cord$_{stat}$ and the cord$_{dyn}$ for each of the 15 BFFE images were calculated (Figures 1C and 1D). The average cord$_{dyn}$ dose, which more closely reflects the real-life situation (Figure 1E) in SBRT delivery, was derived by averaging of cord dose$_{max}$ of each of the 15 images. The maximum cord$_{dyn}$ dose was defined as the maximum of the 15 cord dose$_{max}$ values for each patient.

PTV doses and spinal cord doses were converted to equivalent dose in 2-Gy fraction (EQD2) estimates using the linear-quadratic (LQ) model[2,16] to allow direct comparisons incorporating the number and size of fractions in the different hypofractionated (3- or 5-fraction) regimens. All doses are reported in EQD2. The mean PTV dose of the clinical treatment plans was 43.4 ± 9.6 Gy (for $\alpha/\beta = 10$ Gy). The mean cord$_{stat}$ dose ranged from 23.1 ± 8.5 Gy (for $\alpha/\beta = 3$ Gy) to 28.6 ± 11.9 Gy (for $\alpha/\beta = 0.87$ Gy),[2] and 24.9 ± 8.5 Gy for $\alpha/\beta = 2$ Gy. Cord doses are reported as EQD2 (for $\alpha/\beta = 2$ Gy). Details of the LQ model and EQD2 computations are presented in the **Supplemental Digital Content**.

Quantifying Motion

Dice and Jaccard coefficients were calculated comparing the spinal cord contours in each of the dynamic images (cord$_{dyn}$) with the cord contour in the static T2-weighted image (cord$_{stat}$). Mean and standard deviation of all 15 images were calculated for each patient. Coordinates of the centroids of static and dynamic cord contours were computed. Motion between the 2 images was quantified as the distance between the centroids. Cord$_{stat}$ was used as a fixed reference point for motion assessment.

Statistical Analysis

Statistical analysis was performed using SPSS v19.0 (IBM) and R version 3.1.1 (R Foundation for Statistical Computing, Vienna, Austria). Continuous data were summarized using the median and range. The paired t-test was used to compare the magnitude of cord excursions in different directions. Spearman's rank correlation coefficient was used to examine the relationship between spinal cord motion and changes in dose. For all tests, $P < .05$ was considered statistically significant.

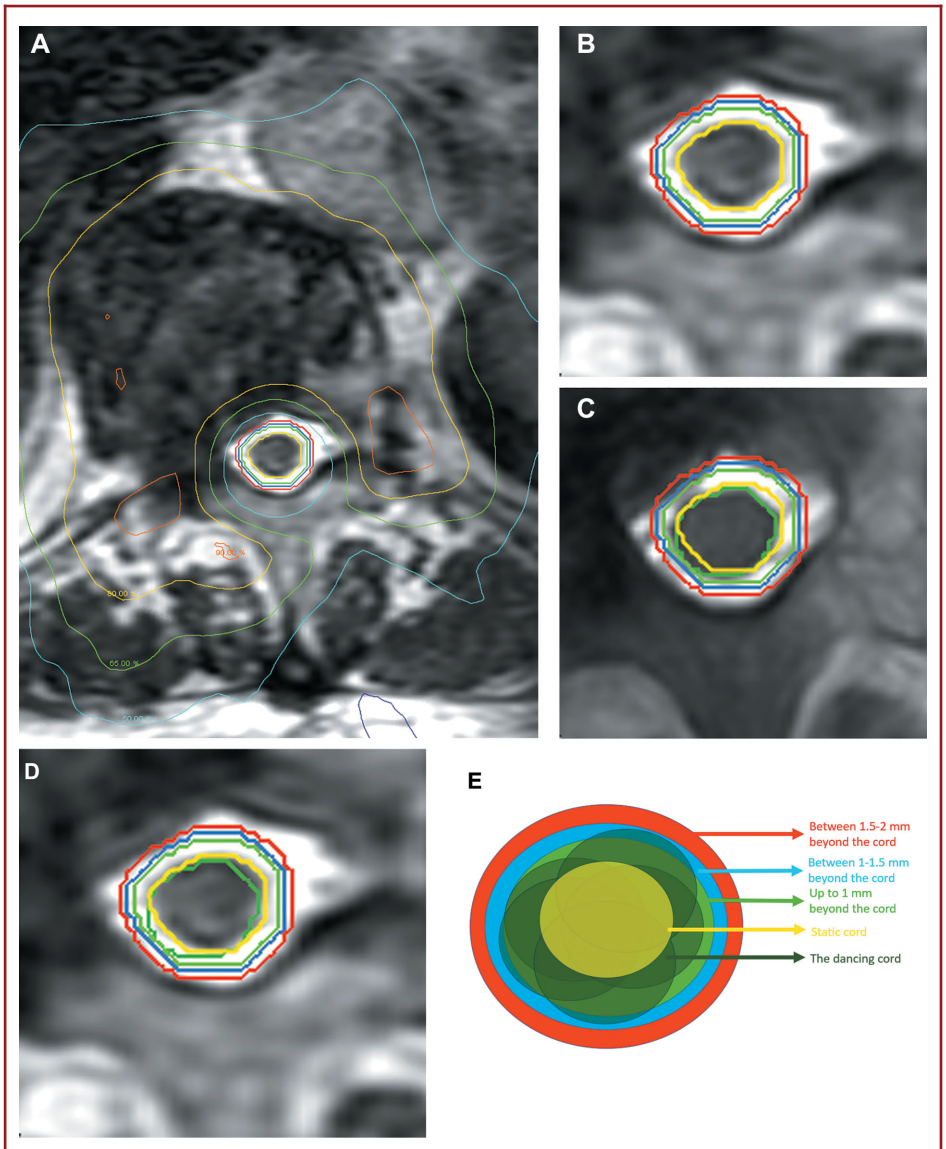

FIGURE 1. *BFFE and spinal cord delineation with PRV margins.* **A**, *Axial static volumetric T2-weighted (DRIVE) image at the level of the spine metastasis with spinal cord delineation and superimposed isodose lines from the SBRT dosimetry (obtained from coregistration with the radiation therapy planning CT, as done in routine dosimetry planning). The isodose lines demonstrate the steep dose gradients in close proximity to the spinal cord.* **B**, *Same T2-weighted image as in* **A**, *magnified and without isodose lines: The static cord ($cord_{stat}$) is contoured in yellow, a 1-mm PRV margin around $cord_{stat}$ in light green, a 1.5-mm margin in blue, and a 2-mm margin in red.* **C**, *BFFE image at the same level as* **A** *and* **B**. *One of $cord_{dyn}$'s motion phases is shown (dark green contour), demonstrating that in this phase, $cord_{dyn}$ excurses to 1 mm from the confines of $cord_{stat}$. The color scheme is the same as in* **A** *and* **B**. **D**, *T2-weighted image (same as in* **B**) *shows $cord_{stat}$, 1, 1.5, and 2-mm margins delineated in the same color scheme as in* **B**, *and demonstrates the motion phase seen in* **C** *where $cord_{dyn}$ (dark green contour) excurses to 1 mm from the confines of $cord_{stat}$.* **E**, *Schematic representation of the "dancing" cord moving in and out of the $cord_{stat}$ and $cord_{stat}$ plus PRV margins. $Cord_{dyn}$, $cord_{stat}$, and the 1, 1.5, and 2-mm margins are shown in same color scheme as in* **A**-**D**. *The schematic illustrates $cord_{dyn}$ excursions in multiple directions during the imaging beyond the 1-mm margin up to the 1.5-mm margin of $cord_{stat}$.*

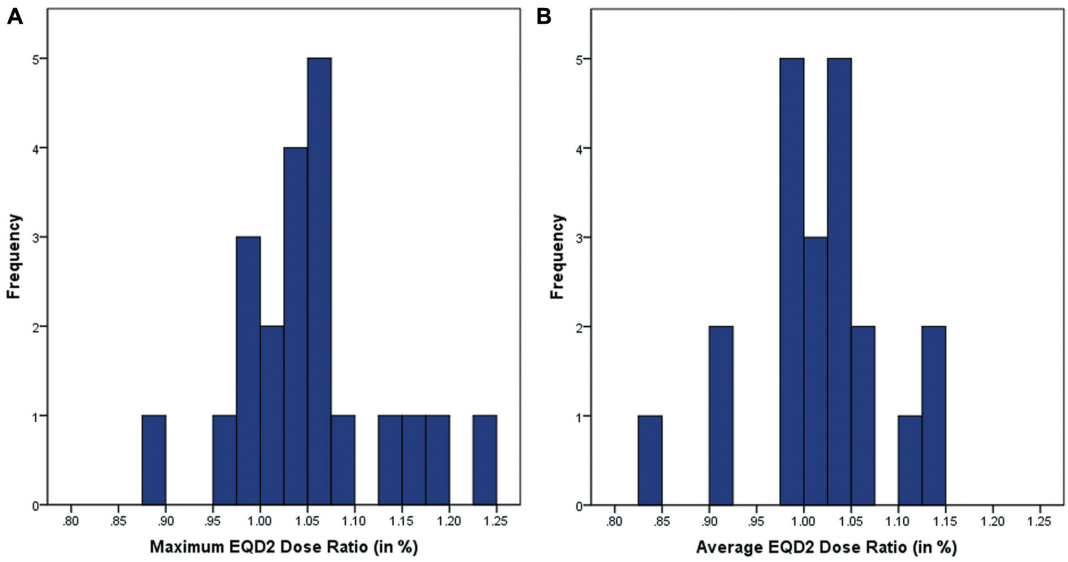

FIGURE 2. *Proportional excess in maximal dose to $cord_{dyn}$. The histogram shows the frequency distribution of the ratio of dose to $cord_{dyn}$ to dose to $cord_{stat}$. The dose ratios are based on EQD2 doses (using an α/β ratio of 2 Gy) to account for differences in the number and size of the fractions used in the SBRT treatments.* **A**, *(left): The histogram shows the frequency distribution of the maximum of dose ratios ($cord_{dyn}/cord_{stat}$) among all dynamic images within each 15-image BFFE imaging study.* **B**, *(right): Frequency distribution of the average of dose ratios ($cord_{dyn}/cord_{stat}$), averaged across all dynamic images within each BFFE study for each patient. The figure demonstrates that average dose ratios were smaller: The dose to $cord_{dyn}$ within each 15-image BFFE study exceeded that of $cord_{stat}$ in 62% of the patients.*

RESULTS

Spinal Cord Dose

The *average* EQD2 dose received by $cord_{dyn}$ exceeded that of $cord_{stat}$ in 13 of the 21 patients (62%) and was lower than the $cord_{stat}$ dose in the remaining 8 patients. The average dose increase of $cord_{dyn}$ over $cord_{stat}$ ranged from 0.6% to 13.8% (median: 4.3%), corresponding to 0.1 to 4.6 Gy (median: 1.0 Gy). The average $cord_{dyn}$ dose exceeded the $cord_{stat}$ dose by >5% in 5 patients (5/21, 24%) and by >10% in 3 patients (3/21, 14%) (Figure 2).

Using the *maximal* $cord_{dyn}$ excursion (among the 15 BFFE images), the maximal $cord_{dyn}$ dose exceeded that of $cord_{stat}$ in 76% of the patients (16/21), was lower in 4 patients, and remained unchanged in 1 patient. The maximal dose increase of $cord_{dyn}$ over $cord_{stat}$ ranged from 1.4% to 23.5% (median: 5.7%) or 0.4 to 7.8 Gy (median: 1.4 Gy). Maximal $cord_{dyn}$ dose exceeded $cord_{stat}$ dose by >5% in 10 patients (10/21, 48%) and by >10% in 4 patients (4/21, 19%) (Figure 2).

Spinal Cord Motion

The degree and frequency distribution of $cord_{dyn}$'s motion with respect to $cord_{stat}$, image by image during BFFE imaging, is presented in Figures 3. The tracing of the $cord_{dyn}$ motion in each patient is illustrated in Figure 4, and a visual representation of the spinal cord motion is shown in the Video. Across the 315 dynamic

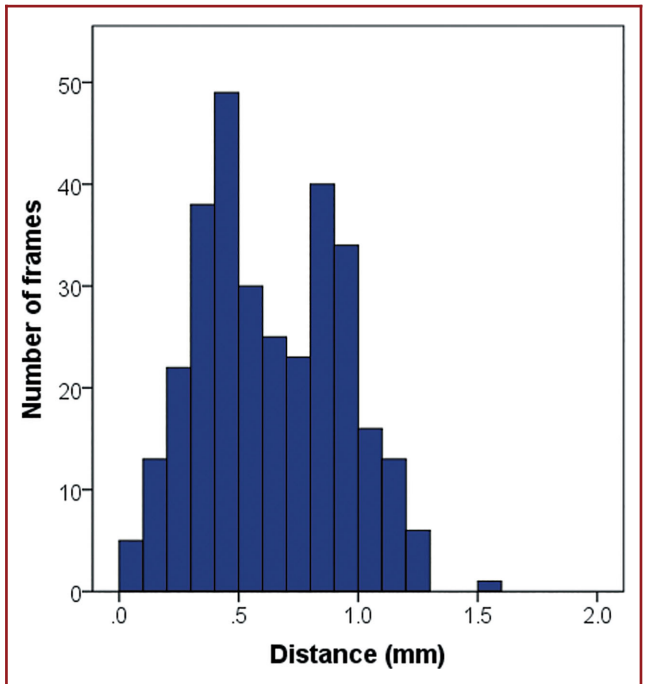

FIGURE 3. *Frequency of $cord_{dyn}$ excursion. The histogram shows the distance (in increments of 0.1 mm) and frequency of spinal $cord_{dyn}$ motion (excursion) beyond the confines of $cord_{stat}$ in the total patient cohort.*

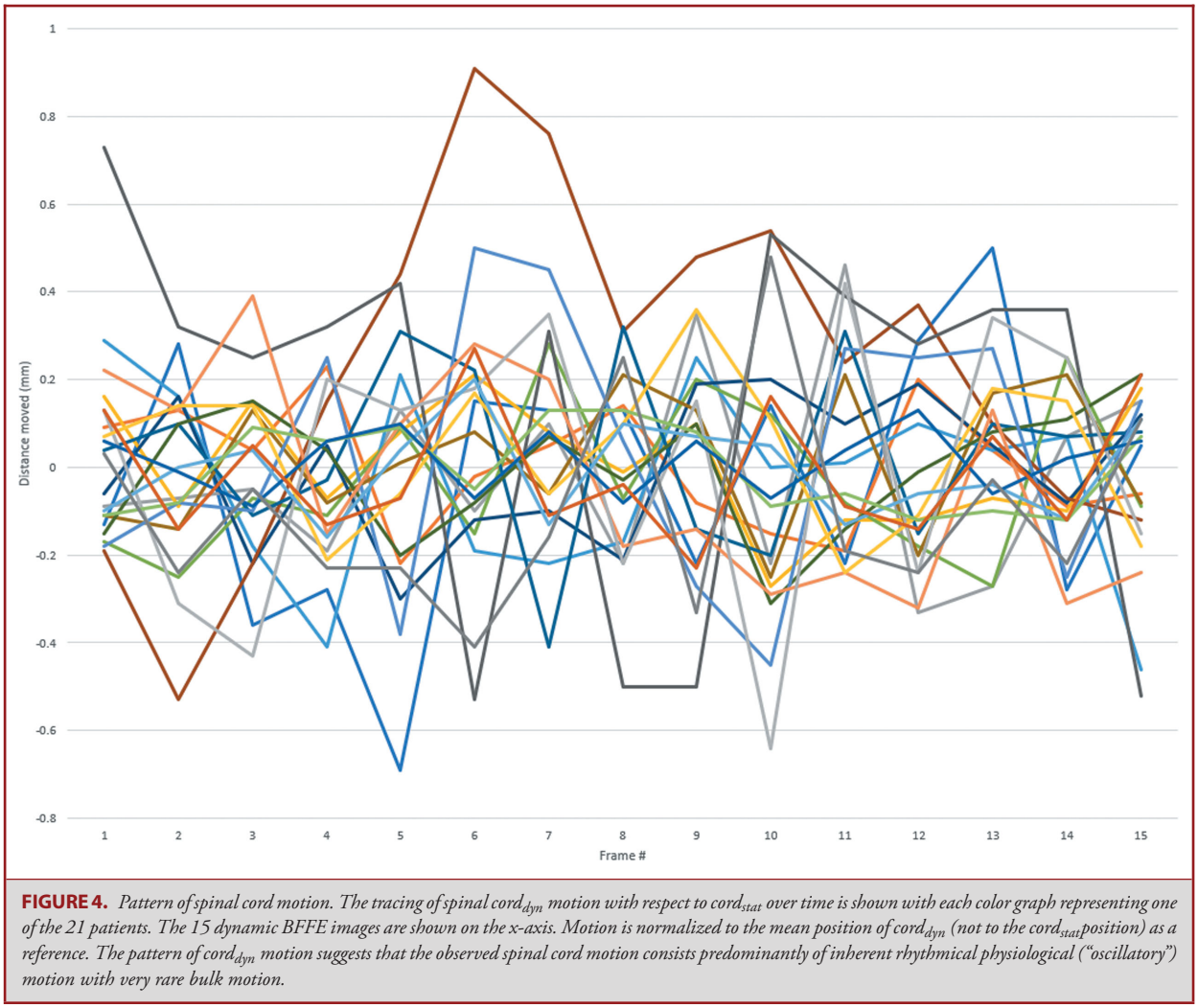

FIGURE 4. *Pattern of spinal cord motion. The tracing of spinal cord$_{dyn}$ motion with respect to cord$_{stat}$ over time is shown with each color graph representing one of the 21 patients. The 15 dynamic BFFE images are shown on the x-axis. Motion is normalized to the mean position of cord$_{dyn}$ (not to the cord$_{stat}$position) as a reference. The pattern of cord$_{dyn}$ motion suggests that the observed spinal cord motion consists predominantly of inherent rhythmical physiological ("oscillatory") motion with very rare bulk motion.*

images (15 images x 21 patients), cord$_{dyn}$ excursions outside cord$_{stat}$ ranged from 0.0 to 1.5 mm (median: 0.6 mm). Dice and Jaccard coefficients of cord$_{dyn}$ and cord$_{stat}$ ranged from 0.70 to 0.95 (median: 0.87) and 0.54 to 0.90 (median: 0.77), respectively. The cord$_{dyn}$ motion in the anteroposterior (AP) direction was significantly greater (median: 0.5 mm, range: 0.1-1.5 mm) than in the lateral direction (median: 0.3 mm, range: 0.0-1.1 mm; $P = .04$). Spinal cord motion of more than 0.5 mm was common and occurred in 86% of the patients (18/21) and 60% of the dynamic images (188/315).

Hypothetical PRV margins of 1, 1.5, and 2 mm surrounding cord$_{stat}$, as often used clinically, were evaluated for their ability to encompass the excursions of cord$_{dyn}$ (as illustrated in Figure 1B, 1D, and 1E). Cord$_{dyn}$ spatially extended outside the volume of cord$_{stat}$ + 1 mm in 43% of the patients (9/21). Of these 9 patients, 7 (78%) had an excess in cord dose. Cord$_{dyn}$ abutted cord$_{stat}$ + 1.5 mm in 1 patient (1 image), but did not extend outside cord$_{stat}$ + 1.5 mm or outside cord$_{stat}$ + 2 mm PRV margin.

Spinal Cord Motion and Dose

The EQD2 dose ratio of cord$_{dyn}$ over cord$_{stat}$ across the 315 dynamic images ranged from 0.9 to 1.2 for maximal cord$_{dyn}$ dose and from 0.9 to 1.1 for average cord$_{dyn}$ dose. We did not identify a clear correlation between the spatial degree/extent of cord$_{dyn}$'s motion (as illustrated in Figures 1C-1E) and the dose received by cord$_{dyn}$ ($r = 0.11$, $P = .55$).

DISCUSSION

While physiological organ motion and its dosimetric consequences have gained much attention in high-precision and stereotactic radiation therapy for many tumor sites,[17-21] spinal cord motion and its impact on spinal cord dose have not been

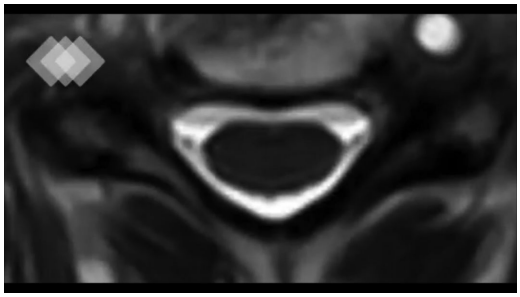

VIDEO. *Cord motion is demonstrated in the dynamic cine-loop images. The video was repeated 4 times to facilitate the visualization of the cord motion. These axial BFFE images were acquired at the single spinal level and included 15 cardiac-gated images with 100 ms temporal resolution during a cardiac cycle. The total imaging time for such a fast acquisition and cardiac gated BFFE image ranges from 2.5 to 5 min, depending on the heart rate, in order to improve the imaging's signal-to-background ratio and provide adequate imaging quality.*

incorporated into dosimetric planning in spine SBRT. BFFE MRI applied in our patients provided cardiac-gating, exquisite cord-cerebrospinal fluid (CSF) contrast, and excellent spatial and temporal resolution for dynamic imaging to assess real-time cord motion in individual patients (see Video).

Key Results

Our results show that physiological spinal cord motion during SBRT results in increases of spinal cord dose in the majority of patients. The proportion of patients with motion-induced dose increase to $cord_{dyn}$ over $cord_{stat}$ was high, both for the average dose excess (62%) and the maximal dose excess (76%, Figure 2). While it is not well established whether the average dose received over time or short intervals of very high maximal dose are more likely to impart neural injury, our results were largely based on the more conservative measure of the *average* dose excess to $cord_{dyn}$.

The observed wide interindividual heterogeneity of the dose excess received by the moving cord (0.6-13.8%, Figure 2) illustrates the challenges to predict motion-induced cord dose increases for individual patients. Such individual heterogeneity may be influenced by random and variable degrees and direction of the cord's motion pattern with respect to the tumor target.

A substantial cord dose excess of 10% or more was seen in 14% of our patients, which is beyond the acceptable range of variation in radiation oncology practice. In clinical practice, dose increase to the spinal cord is expected to have greater impact in severely hypofractionated large-fraction SBRT regimens, where small incremental increases in nominal dose can translate into much higher biological effects, particularly in *single*-fraction regimens.

Interpretation

While a range of α/β ratios (0.87-3 Gy, see **Supplemental Digital Content**) have been reported,[2,16] and the radiosensitivity of the cord may vary at different spinal levels,[22,23] we employed an α/β ratio of 2 Gy, as proposed by HyTEC[24] for all spinal levels. The EQD2 based on the LQ cell survival model interpolation of the maximum tolerated spinal cord dose of 12 Gy in 1 fraction (accepted cord dose constraint for myelopathy in single-fraction regimens) corresponds to 36 Gy ($\alpha/\beta = 3$ Gy) to 53.8 Gy ($\alpha/\beta = 0.87$ Gy) based on the accepted range of α/β between 0.87 and 3 Gy.[2,16] For a *single-fraction* SBRT regimen, a motion-induced cord dose ($cord_{dyn}$) in excess of 10% would correspond to an EQD2 cord dose of 14.9% ($\alpha/\beta = 3$ Gy) to 16.1% ($\alpha/\beta = 0.87$ Gy) higher than the accepted SBRT constraint. These considerations suggest that in situations of expected high cord dose (eg, because of close proximity to the target, and/or diminished cord tolerance from prior radiation), combined with significant cord motion, caution should be exercised to lessen cord motion-induced dose effects by delivering treatments in multiple (3-5 fractions) rather than a single fraction. The impact of spinal cord motion on spinal cord dose may also explain the observation of radiation-induced myelitis that have been reported in single-fraction SBRT regimens after relatively low doses,[11,25] as computation of these cord doses was based on static cord assessments.

To our knowledge, our study is the first investigation to assess the dosimetric effects of spinal cord motion using current high-precision MRI-based delineation of the spinal cord. Radiation dose effects from spinal cord motion in cancer patients have been challenging to evaluate with conventional imaging. MRI and CT myelogram can differentiate the spinal cord from CSF and epidural space, but the intrinsic cord motion assessment has been hampered by limited temporal resolution. We employed BFFE, an advanced dynamic MRI sequence which has the advantage of cardiac gating and provides exquisite spatial resolution and tissue contrast. The only other investigation of dosimetric effects from cord motion by Wang et al[15] studied cord dose with respect to respiratory motion using CT imaging. The investigators reported a 1.5% increase in maximal cord/cauda dose in the worst case in a cohort of 33 spinal metastasis patients. However, because CT imaging cannot reliably differentiate the spinal cord from the surrounding CSF, the spinal canal served as surrogate for the spinal cord position and the assessment of intrinsic cord motion was not possible.

The cause for spinal cord motion is thought to be multifactorial and related to CSF pulsation,[26,27] respiration,[28-32] arterial pulsation,[28,31-34] including the radicular arteries,[35] and biomechanical effects, such as the compliance of the central nervous system.[36] All can contribute to the individual heterogeneity. Existing literature reports oscillatory cord motion to be generally less than 1 mm most of the time in nonmalignant disease and normal individuals; however, the reported values vary, most likely due to different methodologies, patient populations, and small number of cases (Table 3). Our observations on cord motion are overall within the range of previously reported values.[13,15,35,37-43] Tseng et al[13] reported no excursions beyond 1.5 mm caused by physiological oscillatory motion of the spinal cord. While cord motion beyond 1 mm occurred in 43% (9/21) of our patients, no

TABLE 3. Studies Investigating Spinal Cord Motion

Author	Method	No. of cases	Motion (mm)	Comments
Oncology patients				
Oztek et al, 2020 (current study)	Cine MRI	21 lesions in 21 patients	0.1-1.5 mm, median 0.6 mm (AP) 0-1.1 mm, median 0.5 mm (LR) 0-1.5 mm, median 0.3 mm (total)	Spine metastasis patients
Wang et al,[15] 2016	CT	33 lesions in 30 patients[a]	4 cases $\leq$ 0.2 (AP) 2 cases $\leq$ 0.2 (LR) 8 cases $\leq$ 0.6 (CC)[b]	Lung cancer patients Spinal canal motion
Tseng et al,[13] 2015	Cine MRI	74	0.12-0.39 (AP) 0.13-0.41 (LR) 0.29-0.77 (CC)	Spine metastasis patients
Cai et al,[37] 2007	Cine MRI	7	Total motion typically <0.5	Lung cancer patients with normal spine (4); healthy volunteers (3) T spine. Mean total motion
Nononcology pathologies				
Vavasour et al[38] 2014[c]	Phase-contrast MRI	13 + 15[d]	0.02-2.64 mm (spondylotic myelopathy)[d] 0.03-0.54 (controls)[d] (CC)	Chronic spondylosis patients (13); controls (15)
Healthy volunteers				
Winklhofer et al,[39] 2014	Cine MRI	16	0.06-1.7	Healthy volunteers
Figley et al,[40] 2008	Cine MRI	8	0.36 $\pm$ 0.13 (AP) 0.15 $\pm$ 0.07 (LR)	Healthy volunteers Lower T-, L-, sacral spine
Figley et al,[41] 2007	Cine MRI	10	0.72 $\pm$ 0.33/0.46 $\pm$ 0.32 (AP)[e] 0.17 $\pm$ 0.09 (LR)	Healthy volunteers
Mikulis et al,[42] 1994[c]	Phase-contrast MRI	11	0.4-0.5 (CC)	Healthy volunteers
Enzmann et al,[43] 1992[c]	Phase-contrast MRI	10	0.22 $\pm$ 0.06 (CC)	Healthy volunteers Upper C-spine
Animal studies				
Matsuzaki et al,[35] 1996[f]	M-mode ultrasound	5[f]	0.080 $\pm$ 0.1132 (AP)[f]	Canines

AP = anteroposterior; CC = craniocaudal; LR = left right.
[a]In this study, 23 lesions did not demonstrate any motion.
[b]In this study, 6 cases had CC motion $\leq$ 0.2 mm and only 2 cases had 0.2 to 0.6 mm motion.
[c]Motion calculated from velocity data.
[d]This study presents data separately for patients with chronic spondylotic myelopathy and the control group.
[e]AP motion data were provided separately for patients with straight spine and curved spine, because a significant difference between the 2 groups was demonstrated.
[f]This study was conducted on 10 dogs, where cord motion was observed in only 5. The data provided are based on the 5 dogs with observed cord motion before any interventions on the cord were performed. Data in micrometers were converted to mm for this table.

excursion beyond 1.5 mm was seen, confirming the results from Tseng et al.[13]

Generalizability and Implications for Practice

Our results are generalizable to the treatment of patients with metastatic spinal lesions with respect to the PRV margin for the spinal cord in SBRT planning. Based upon the overall consistency of our cord motion findings with the literature,[13,15,35,37-43] the unlikely excursion of the cord beyond 1.5 to 2 mm from its static position, and our observed dosimetric effects of spinal cord motion, we recommend to employ a 1.5 to 2 mm margin for the spinal cord PRV in SBRT dosimetry planning to mitigate motion-related dose effects from the "dancing" cord. Our data also suggest that a 1-mm PRV margin is inadequate based on our observation that the cord moves beyond 1 mm of its static position in nearly half (43%) of the patients and that 78% of these showed a motion-induced excess in cord dose.

In challenging cases, where the spinal cord is anticipated to closely approach the cord constraint, a dynamic motion study of the cord can be easily obtained with an added approximately 2.5- to 5-min dynamic MRI sequence to provide additional guidance.

Limitations

Our patient and lesion numbers were limited, which did not allow meaningful subgroup analyses, such as associations of cord motion and dose with lesion size, spinal level, extent of

vertebral involvement, Bilsky grade, or patient-related variables, such as coexisting spine pathologies.[42] Assessment of these factors may enable a more patient-tailored approach. Our study is a physics/dosimetry and imaging assessment of motion-induced changes in spinal cord dose, and our cohort is too small to correlate the observed dosimetric findings with clinical myelopathy. Further, while our 2.5- to 5-min imaging time readily assesses physiological motion, it may not capture all bulk motion that may occur during a typical SBRT fraction delivery.

Additionally, the BFFE images were obtained only in the axial plane, which did not allow assessment of craniocaudal cord motion that has been reported as larger than AP and lateral motion.[13,15] However, the target and cord are usually assessed and contoured in the axial plane. Thus, we believe that the effects of craniocaudal cord motion on the critical cord–target distance have likely been incorporated, at least in part, in the dose calculations derived from the axial dynamic BFFE images.

CONCLUSION

Our preliminary study and dosimetry findings show that spinal cord motion contributes measurable, variable, and potentially detrimental dose effects to the cord in patients treated with SBRT for spine metastasis. We recommend a 1.5- to 2-mm cord PRV margin based on the observed motion properties of the spinal cord and the dose effects from the cord motion. If available, a short dynamic cardiac-gated MRI may be also considered to quantify spinal cord motion. Future studies are required to reconfirm our results.

Disclosures

The authors have no personal, financial, or institutional interest in any of the drugs, materials, or devices described in this article.

REFERENCES

1. Klimo P Jr, Schmidt MH. Surgical management of spinal metastases. *Oncologist*. 2004;9(2):188-196.
2. Kirkpatrick JP, van der Kogel AJ, Schultheiss TE. Radiation dose-volume effects in the spinal cord. *Int J Radiat Oncol Biol Phys*. 2010;76(3 Suppl):S42-S49.
3. Tseng CL, Eppinga W, Charest-Morin R, et al. Spine stereotactic body radiotherapy: indications, outcomes, and points of caution. *Global Spine J*. 2017;7(2):179-197.
4. Lo SS, Chang EL, Ryu S, et al. Best of International Stereotactic Radiosurgery Society Congress 2013: stereotactic body radiation therapy. Part I: spinal tumors. *Future Oncol*. 2013;9(9):1299-1302.
5. Sahgal A, Ma L, Gibbs I, et al. Spinal cord tolerance for stereotactic body radiotherapy. *Int J Radiat Oncol Biol Phys*. 2010;77(2):548-553.
6. De Bari B, Alongi F, Mortellaro G, Mazzola R, Schiappacasse L, Guckenberger M. Spinal metastases: is stereotactic body radiation therapy supported by evidences? *Crit Rev Oncol Hematol*. 2016;98:147-158.
7. Huo M, Sahgal A, Pryor D, Redmond K, Lo S, Foote M. Stereotactic spine radiosurgery: review of safety and efficacy with respect to dose and fractionation. *Surg Neurol Int*. 2017;8:30.
8. Ma L, Sahgal A, Hossain S, et al. Nonrandom intrafraction target motions and general strategy for correction of spine stereotactic body radiotherapy. *Int J Radiat Oncol Biol Phys*. 2009;75(4):1261-1265.
9. van Mourik AM, Sonke JJ, Vijlbrief T, et al. Reproducibility of the MRI-defined spinal cord position in stereotactic radiotherapy for spinal oligometastases. *Radiother Oncol*. 2014;113(2):230-234.
10. Emami B, Lyman J, Brown A, et al. Tolerance of normal tissue to therapeutic irradiation. *Int J Radiat Oncol Biol Phys*. 1991;21(1):109-122.
11. Katsoulakis E, Jackson A, Cox B, Lovelock M, Yamada Y. A detailed dosimetric analysis of spinal cord tolerance in high-dose spine radiosurgery. *Int J Radiat Oncol Biol Phys*. 2017;99(3):598-607.
12. Redmond KJ, Lo SS, Soltys SG, et al. Consensus guidelines for postoperative stereotactic body radiation therapy for spinal metastases: results of an international survey. *J Neurosurg Spine*. 2017;26(3):299-306.
13. Tseng CL, Sussman MS, Atenafu EG, et al. Magnetic resonance imaging assessment of spinal cord and cauda equina motion in supine patients with spinal metastases planned for spine stereotactic body radiation therapy. *Int J Radiat Oncol Biol Phys*. 2015;91(5):995-1002.
14. Hyde D, Lochray F, Korol R, et al. Spine stereotactic body radiotherapy utilizing cone-beam CT image-guidance with a robotic couch: intrafraction motion analysis accounting for all six degrees of freedom. *Int J Radiat Oncol Biol Phys*. 2012;82(3):e555-e562.
15. Wang X, Ghia AJ, Zhao Z, et al. Prospective evaluation of target and spinal cord motion and dosimetric changes with respiration in spinal stereotactic body radiation therapy utilizing 4-D CT. *J Radiosurg SBRT*. 2016;4(3):191-201.
16. Bentzen SM, Joiner MC. The linear-quadratic approach in clinical practice. In: Joiner MC, Kogel AJ, eds. *Basic Clinical Radiobiology*. 5th ed. Boca Raton: CRC Press; 2018.
17. Admiraal MA, Schuring D, Hurkmans CW. Dose calculations accounting for breathing motion in stereotactic lung radiotherapy based on 4D-CT and the internal target volume. *Radiother Oncol*. 2008;86(1):55-60.
18. Jin JY, Ajlouni M, Chen Q, Kong FM, Ryu S, Movsas B. Quantification of incidental dose to potential clinical target volume (CTV) under different stereotactic body radiation therapy (SBRT) techniques for non-small cell lung cancer - tumor motion and using internal target volume (ITV) could improve dose distribution in CTV. *Radiother Oncol*. 2007;85(2):267-276.
19. Li H, Chang JY. Accounting for, mitigating, and choice of margins for moving tumors. *Semin Radiat Oncol*. 2018;28(3):194-200.
20. Xie T, Zaidi H. Effect of respiratory motion on internal radiation dosimetry. *Med Phys*. 2014;41(11):112506.
21. Yang M, Timmerman R. Stereotactic ablative radiotherapy uncertainties: delineation, setup and motion. *Semin Radiat Oncol*. 2018;28(3):207-217.
22. Adamus-Gorka M, Brahme A, Mavroidis P, Lind BK. Variation in radiation sensitivity and repair kinetics in different parts of the spinal cord. *Acta Oncol*. 2008;47(5):928-936.
23. Kramer S, Lee KF. Complications of radiation therapy: the central nervous system. *Semin Roentgenol*. 1974;9(1):75-83.
24. Sahgal A, Chang JH, Ma L, et al. Spinal cord dose tolerance to stereotactic body radiation therapy *Int J Radiat Oncol Biol Phys*. published online: October 10, 2019 (doi:10.1016/j.ijrobp.2019.09.038).
25. Sahgal A, Weinberg V, Ma L, et al. Probabilities of radiation myelopathy specific to stereotactic body radiation therapy to guide safe practice. *Int J Radiat Oncol Biol Phys*. 2013;85(2):341-347.
26. Du Boulay G, O'Connell J, Currie J, Bostick T, Verity P. Further investigations on pulsatile movements in the cerebrospinal fluid pathways. *Acta Radiol Diagn (Stockh)*. 1972;13(2):496-523.
27. Du Boulay GH. Pulsatile movements in the CSF pathways. *Br J Radiol*. 1966;39(460):255-262.
28. Brezner A, Kay B. Spinal cord ultrasonography in children with myelomeningocele. *Dev Med Child Neurol*. 1999;41(7):450-455.
29. Friese S, Hamhaber U, Erb M, Kueker W, Klose U. The influence of pulse and respiration on spinal cerebrospinal fluid pulsation. *Invest Radiol*. 2004;39(2):120-130.
30. Schroth G, Klose U. Cerebrospinal fluid flow. II. Physiology of respiration-related pulsations. *Neuroradiology*. 1992;35(1):10-15.
31. Schumacher R, Richter D. One-dimensional Fourier transformation of M-mode sonograms for frequency analysis of moving structures with application to spinal cord motion. *Pediatr Radiol*. 2004;34(10):793-797.
32. Wolf K, Hupp M, Friedl S, et al. In cervical spondylotic myelopathy spinal cord motion is focally increased at the level of stenosis: a controlled cross-sectional study. *Spinal Cord*. 2018;56(8):769-776.
33. Tanaka H, Sakurai K, Iwasaki M, et al. Craniocaudal motion velocity in the cervical spinal cord in degenerative disease as shown by MR imaging. *Acta Radiol*. 1997;38(5):803-809.
34. Zieger M, Dorr U. Pediatric spinal sonography. Part I: anatomy and examination technique. *Pediatr Radiol*. 1988;18(1):9-13.

35. Matsuzaki H, Wakabayashi K, Ishihara K, Ishikawa H, Kawabata H, Onomura T. The origin and significance of spinal cord pulsation. *Spinal Cord*. 1996;34(7):422-426.
36. Levy LM, Di Chiro G, McCullough DC, Dwyer AJ, Johnson DL, Yang SS. Fixed spinal cord: diagnosis with MR imaging. *Radiology*. 1988;169(3):773-778.
37. Cai J, Sheng K, Sheehan JP, Benedict SH, Larner JM, Read PW. Evaluation of thoracic spinal cord motion using dynamic MRI. *Radiother Oncol*. 2007;84(3):279-282.
38. Vavasour IM, Meyers SM, MacMillan EL, et al. Increased spinal cord movements in cervical spondylotic myelopathy. *Spine J*. 2014;14(10):2344-2354.
39. Winklhofer S, Schoth F, Stolzmann P, et al. Spinal cord motion: influence of respiration and cardiac cycle. *Rofo*. 2014;186(11):1016-1021.
40. Figley CR, Yau D, Stroman PW. Attenuation of lower-thoracic, lumbar, and sacral spinal cord motion: implications for imaging human spinal cord structure and function. *AJNR Am J Neuroradiol*. 2008;29(8):1450-1454.
41. Figley CR, Stroman PW. Investigation of human cervical and upper thoracic spinal cord motion: implications for imaging spinal cord structure and function. *Magn Reson Med*. 2007;58(1):185-189.
42. Mikulis DJ, Wood ML, Zerdoner OA, Poncelet BP. Oscillatory motion of the normal cervical spinal cord. *Radiology*. 1994;192(1):117-121.
43. Enzmann DR, Pelc NJ. Brain motion: measurement with phase-contrast MR imaging. *Radiology*. 1992;185(3):653-660.

Supplemental digital content is *available for this article at www.neurosurgery-online.com.*

Supplemental Digital Content. EQD2 computations and linear-quadratic (LQ) model. Details of EQD2 computations and LQ model.